JOURNAL OF MATERIALS SCIENCE **38** (2003) 2647–2654

The deformation and fracture behavior of SiCw/AZ91 magnesium matrix composite during *in-situ* TEM straining

M. Y. ZHENG
School of Materials Science and Engineering, Harbin Institute of Technology, Harbin 150001, People's Republic of China; Department of Mechanical Engineering, Nagaoka University of Technology, Nagaoka 940-2188, Japan
E-mail: zheng@stn.nagaokaut.ac.jp

W. C. ZHANG, K. WU, C. K. YAO
School of Materials Science and Engineering, Harbin Institute of Technology, Harbin 150001, People's Republic of China

The deformation and fracture behavior of as-solutionized SiCw/AZ91 magnesium matrix composite was observed during the *in-situ* tensile straining in a transmission electron microscope. The results indicated that the dislocation slip was impeded by the SiC whiskers, a large number of dislocation pile-ups occurred around the whiskers. Microcracks nucleated predominately at the SiC whisker rich regions and the matrix near SiCw-AZ91 interfaces. The SiC whiskers and twins prohibited the crack propagation. The microcracks linked with each other and connected with the main crack, leading to the catastrophic failure of the composite. The fracture processes of the composite were found to be matrix-controlled. The poor ductility of the composite was attributed to the low inherent ductility of the magnesium alloy matrix and the local stress concentration because of the addition of the SiC whiskers.

1. Introduction

Discontinuously reinforced metal matrix composites have a number of advantages over monolithic metallic materials, such as high specific strength and stiffness, increased creep and wear resistance, which make them very attractive materials in aerospace, aircraft and automobile industries. However, the commercial application of these materials is severely restricted by their low ductility and fracture toughness, which stem from the presence of brittle ceramic reinforcement within a ductile matrix. Thus, study of the failure mechanism of these materials has become a research priority in recent years [1–19].

The experimental characterization of the failure of the composites can be achieved by serial sectioning or by fractographic analysis of broken samples [1–3]. This provides valuable information on the damage mechanisms occurring in the bulk of the material, but very limited indication on the chronology of the damage events. Because many mechanisms are involved in failure of the metal matrix composites, it is difficult to identify the dominant one and the contributions made by each through the techniques mentioned above. This problem can be overcome by performing *in situ* characterization of failure during mechanical tests, such as in scanning electron microscope (SEM) [4–7] and transmission electron microscope (TEM) [8–10]. *In-situ* SEM and TEM tensile techniques can provide dynamic observation of the crack initiation and propagation. *In-situ* SEM tensile technique can only be used to observe the changes of surface microstructure, while *in-situ* TEM straining technique can give more information, such as the emission and motion of dislocations in the process of deformation, sites of crack initiation, crack propagation path, as well as the effect of interface and inclusions on the crack initiation and propagation. Although these techniques have given some very interesting results on the sequence of damage leading to the ultimate failure, it has been suggested that the complex stress state which prevails at the surface of the samples where *in situ* observation is performed may bias the determination of the damage mechanisms occurring in the bulk materials [7]. Therefore, the validity of such *in situ* observations with respect to the bulk damage mechanisms has to be checked.

Extensive researches have been carried out on the deformation and fracture behavior of discontinuously reinforced aluminum matrix composites with the above techniques. These studies have concluded that failure mechanisms are highly sensitive to the distribution, morphology and size of reinforcement [1, 11], matrix properties [4], the nature of matrix-reinforcement interface [3, 12], fabrication method of the composites [2], and load condition [3]. These mechanisms can be broadly divided into three classes [13]: reinforcement cracking; matrix-reinforcement decohesion;

matrix ductile failure. The type of predominant damage for a particular composite can be either one or combination of the types, depending on the microstructure of the material and the external load applied.

Through these extensive investigations, a clear understanding of failure behavior in discontinuously reinforced aluminum matrix composites has begun to be achieved. However, little research [14–19] has been carried out on the deformation and fracture behavior of discontinuously reinforced magnesium matrix composites, irrespective of their lower density, superior specific properties and high damping capacity [20–26]. The field emission scanning electron microscope (FE-SEM) fractographs of SiCw/AE42 magnesium composite [14] indicates that the fracture occurs by cracks which propagate from the whisker/matrix interface debonded at whiskers ends to matrix at temperatures lower than 473 K. Martin has investigated the failure mechanism of SiCp/Mg-6%Zn composite in tension and fully reversed cyclic deformation using quantitative SEM [18]. Porosity and inability of the matrix alloy to accommodate large strain gradients induced by the presence of the SiC particles are identified as the main causes of the poor ductility and toughness of the composite. The micromechanism of the crack initiation and propagation in AZ91 alloy reinforced with alumina short fiber and SiC particle has been examined using controlled fracture specimens by SEM [17]. It is indicated that the failure mechanism is mainly controlled by the matrix of the composites. Sohn [19] has investigated the microfracture process in squeeze cast magnesium matrix composites by *in-situ* SEM fracture test. Microcracks are initiated mainly at the fiber/matrix interface at considerably higher stress intensity factor levels. Unfortunately, the previous researches are mainly based on the results of scanning electron microscopy observation, and the details of the deformation and fracture process, such as the dislocation activity, the effect of reinforcement, grain boundaries and twins can hardly be observed.

The purpose of this paper is to investigate the deformation and fracture behavior of SiCw/AZ91 magnesium matrix composite using *in-situ* TEM straining technique. Solution heat treatment (T4) SiCw/AZ91 composite is used because a T4 treatment is quite effective in increasing tensile ductility of the SiC/AZ91 composite without sacrificing the yield strength [24], so that more information can be obtained during the *in-situ* deformation and fracture process.

2. Experimental procedures

The material used in this study was a SiCw/AZ91 magnesium matrix composite fabricated by a squeeze casting method. The β-SiC whiskers were fabricated into a preform by wet forming method. The volume fraction of whisker in the perform was about 0.2. The perform was subsequently infiltrated by molten AZ91 magnesium alloy under a high pressure in a squeeze casting press. Prior to infiltration, the mold and the preform were preheated at 500°C, and AZ91 magnesium melt superheated to 800°C was poured over the perform. The pressure exerted by the punch on the molten metal was gradually increased to a pre-determined level of 100 MPa in order to avoid the deformation of the preform, and the pressure was kept at this level for 3 min until the molten metal was completely solidified.

The composite was subjected to solution heat treatment (T4) at 380°C for 2 h and then at 415°C for 24 h followed by water quenching at 25°C [27].

In-situ TEM tensile specimens with dimension of 3×5 mm^2 were prepared from the solution treated composite. After mechanical polishing, they were dimpled and ion milled to perforation. A liquid nitrogen cold stage was used to limit heat-induced artifacts during the ion milling process. Tensile straining was carried out in an Hitachi H-800 transmission electron microscope equipped with a strain stage. The TEM was operated at 175 kV.

In order to compare the microscopic observation with the bulk material properties, monotonic tension tests were also conducted using dog bone-shaped tensile specimens with 15 mm gauge length and 2 mm thickness on an Instron testing machine. Fractographic observation of the broken samples was carried out in a Hitachi S-570 scanning electron microscope.

3. Experimental results

3.1. SEM fractographs of SiCw/AZ91 composite

Room-temperature tensile properties of AZ91 magnesium alloy and SiCw/AZ91 composite are shown in Table I. The yield strength, ultimate tensile strength and elastic modulus of SiCw/AZ91 composite are significantly higher than those of the unreinforced AZ91 alloy, while the composite exhibits quite lower ductility. A solution heat treatment (T4) produces an obvious increase in tensile ductility of the AZ91 alloy and SiCw/AZ91 composite by dissolving the brittle $Mg_{17}Al_{12}$ phase in the matrix.

Fig. 1 shows the SEM fractographs of SiCw/AZ91 composite under solution treated condition. The fracture process is very localized, no apparent necking is observed. The composite exhibits a mixed mode of brittle feature with limited dimple-like ductile fracture. The dimples are small and shallow, consistent with the quite low ductility of the composite. In the fracture surface, the quantity of the exposed whiskers is far smaller than the volume fraction of SiC whisker in the composite. There is no indication of fracture of SiC whisker. No debonded interface between SiC whisker and magnesium matrix can be observed, indicating a high interfacial bond strength.

TABLE I Tensile properties of AZ91 alloy and SiCw/AZ91 composite

Material	0.2% proof stress ($\sigma_{0.2}$, MPa)	UTS (σ_b, MPa)	Young's modulus (E, GPa)	Elongation to failure (ε, %)
AZ91 (as-cast)	102	205	46	6.00
AZ91 (T4)	87	189	46	8.14
SiCw/AZ91 (as-cast)	240	370	86	0.92
SiCw/AZ91 (T4)	220	355	85	1.40

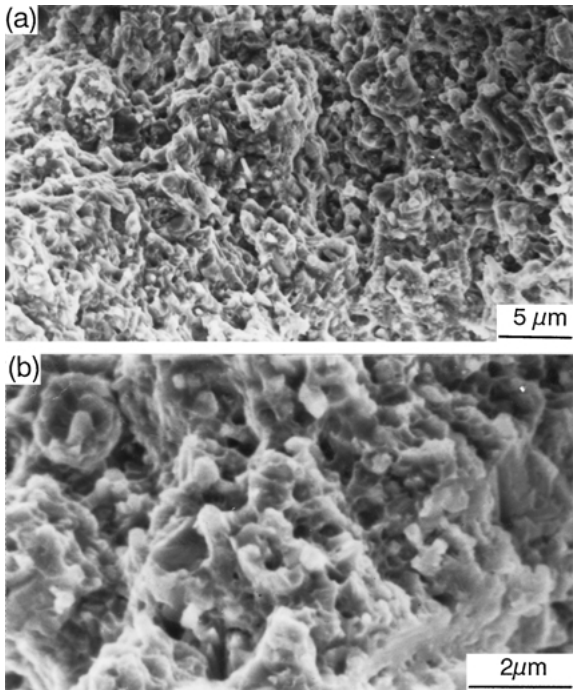

Figure 1 SEM fractographs of solution treated SiCw/AZ91 composites. (a) Lower magnification and (b) higher magnification.

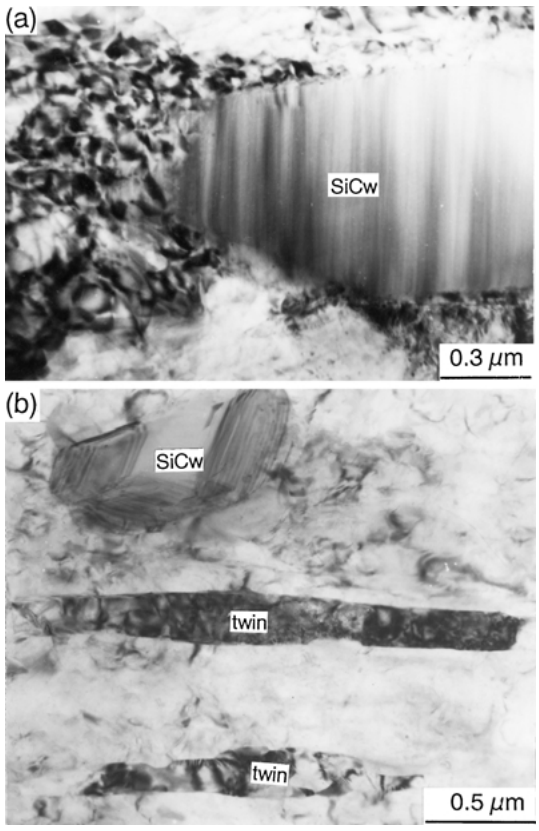

Figure 2 (a) Dislocations and (b) twins in the solution-treated SiCw/AZ91 composite before straining.

3.2. Dislocations activity during *in-situ* TEM straining

Prior to straining, a high density of dislocations can be found in the solution treated SiCw/AZ91 composite, as shown in Fig. 2a. The distribution of the dislocations within the composite is not uniform, there is higher density near the whisker. The high dislocation density is due to the large difference in coefficients of thermal expansion (CTE) between SiC whisker (5×10^{-6} K^{-1}) [28] and AZ91 alloy (26×10^{-6} K^{-1}) [29]. This thermal mismatch will result in substantial stress in the matrix around SiC whisker during cooling from the solutionization temperature, and dislocations are introduced in the composite matrix, especially, in the vicinity of the SiC whiskers [30]. More dislocations are generated at the ends of the SiC whiskers where plastic straining during cooling is greatest, than at the middle of the whisker length.

Magnesium is a hexagonal close-packed structure with limited number of slip systems available for plastic deformation, the stress concentration in the composite is not easy to relieve and twins can be observed. Fig. 2b shows the twins in the matrix of the SiCw/AZ91 composite. The twins belong to $\{10\bar{1}2\}\langle 10\bar{1}1\rangle$, the twin plane is $\{10\bar{1}2\}$.

As the thin foil is loaded, cracks initiate at the edge of the perforation perpendicular to the tensile direction because of stress concentration. Dislocations are emitted at the crack tip, moving ahead quickly. At the same time, the original dislocations existing in the matrix also move ahead. Thus, the local thinning and the dislocation free zone (DFZ) occur in front of the crack tip, as shown in Fig. 3a. When the emitting dislocations meet the SiC whisker ahead, the dislocations are impeded, forming a dislocation pile up at the SiCw-AZ91 interface. At the same time, the crack tip blunts. After further loading, the blunted crack splits again, and the piled-up dislocations at the interface initiate, with the moving direction perpendicular to the original direction, as shown in Fig. 3b.

When dislocations emitting from crack tip meet the whisker ahead with small size, the dislocations can be observed to branch by separating into two paths, bypass the whisker, as shown in Fig. 4. At the same time, the dislocations are also generated at the SiCw-AZ91 interface during straining, these dislocations slip in the matrix, and finally will be impeded by the nearby whiskers, forming a dislocation pile up or bypassing the whisker.

3.3. Initiation of microcracks

After further loading, local thinning appears to occur in the composite. Local thinning regions will develop into microcracks as load increases. Local thinning and microcracks are mainly formed in the matrix in the vicinity of the SiCw-AZ91 interface, as shown in Fig. 5a, and at the whiskers-rich regions, as shown in Fig. 5b. Dislocations are observed to stack in the local thinning regions.

3.4. Growth of cracks

Microcracks will propagate when the applied stress increases to a critical value. Fig. 6 shows a crack meeting a twin in the matrix of the composite. The twin is $\{10\bar{1}2\}\langle 10\bar{1}1\rangle$. When the crack approaches the twin, high stress concentration may develop in the nearby region of the twin, local thinning occurs near the twin-matrix boundary, as shown in Fig. 6a. On

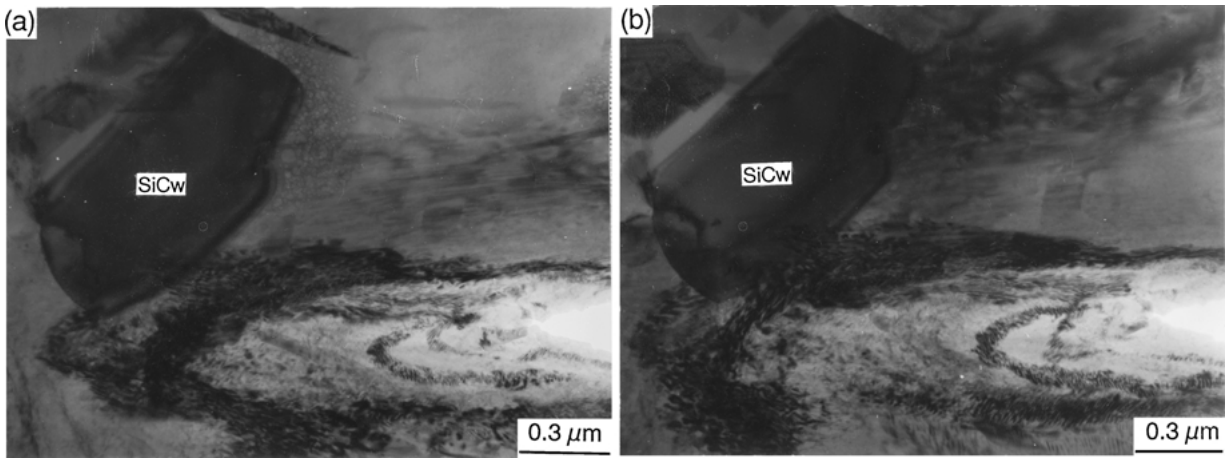

Figure 3 Interaction between dislocations and SiC whisker. (a) Pile up of dislocations at interface and (b) motion of dislocations after further straining.

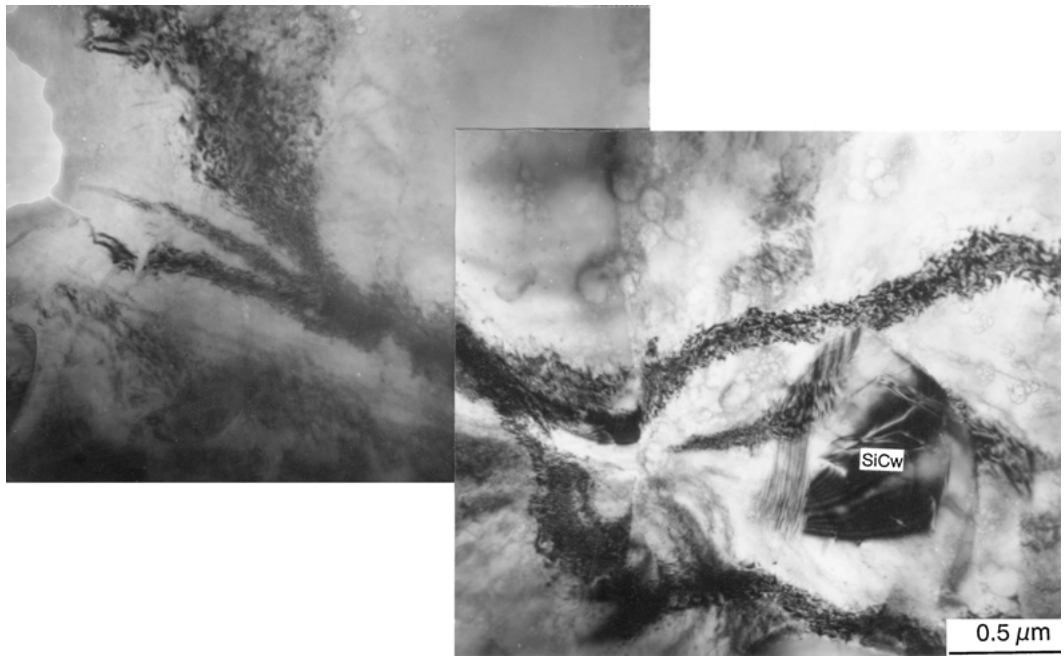

Figure 4 Interaction between dislocations and SiC whisker.

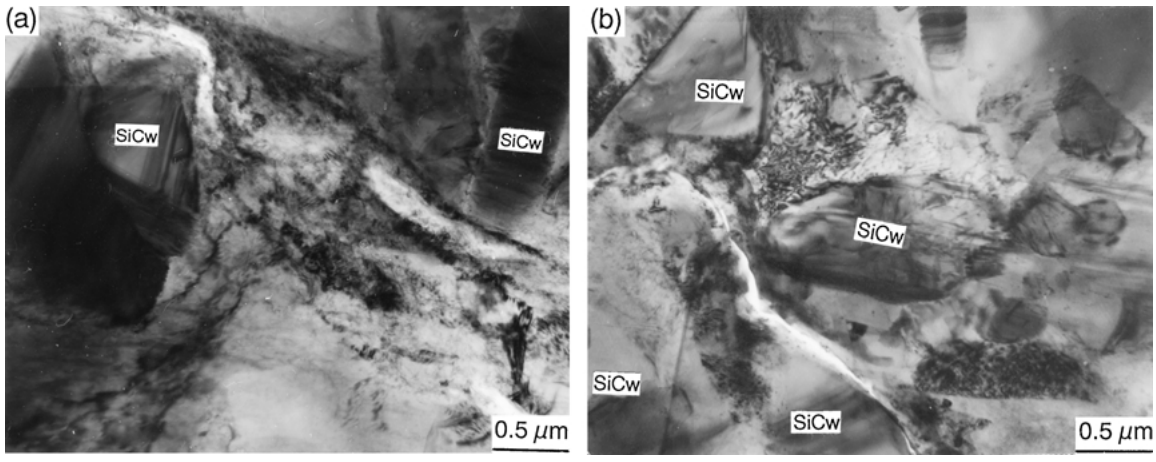

Figure 5 Initiation of micro-cracks in SiCw/AZ91 Mg composite. (a) At the whisker end and (b) in the whisker-rich region.

further loading, crack tip blunts, the local thinning zone is extended, microcrack initiates in the vicinity of the twin boundary, as shown in Fig. 6b. On further straining, main crack connects with the microcrack ahead, and the main crack changes its path into a direction along the twin-matrix interface, as shown in Fig. 6c.

When a crack meets a whisker which is parallel to the crack, it propagates along the whisker-matrix interface, as shown in Fig. 7. It can be observed clearly that there

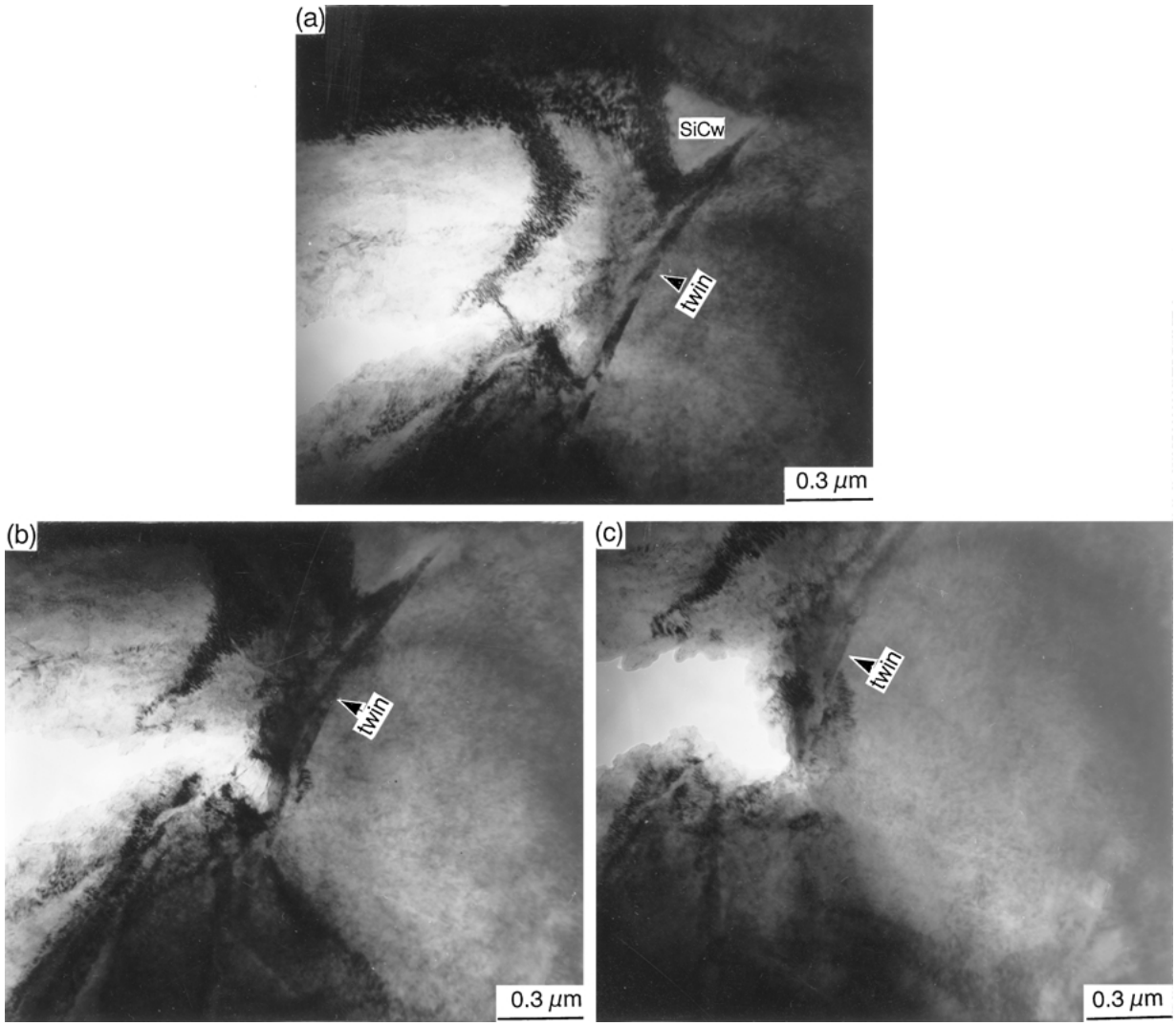

Figure 6 Interaction between crack and twin. (a) Local thinning near twin, (b) initiation of microcrack and (c) propagation of the crack.

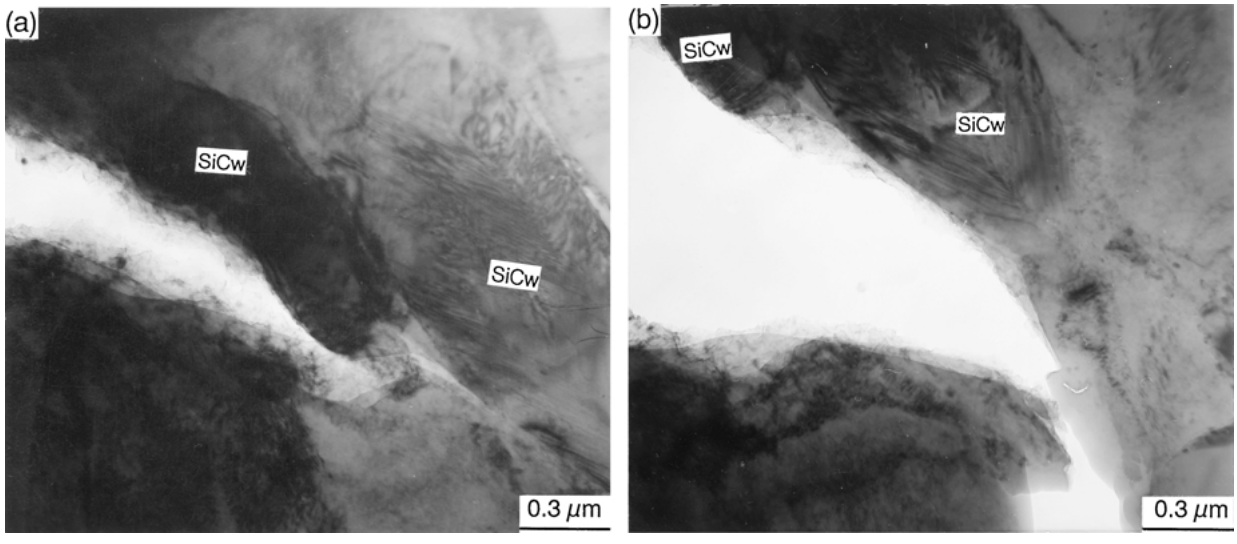

Figure 7 Interaction between crack and SiC whisker. (a) Crack meeting a SiC whisker and (b) crack propagating along the matrix near interface.

exists a layer of magnesium alloy at the surface of SiC whisker, suggesting that the crack propagates in the matrix near the interface.

When a crack meets a whisker which is perpendicular to the crack, it blunts at the whisker-matrix interface, and microcrack initiates at the matrix at the other side of the SiC whisker, as shown in Fig. 8a. On further straining, the cracks connect, and the whisker is pulled out, as shown in Fig. 8b.

Usually more than one dominant crack propagates through the thin foil in direction approximately perpendicular to the applied tensile stress. Some of the

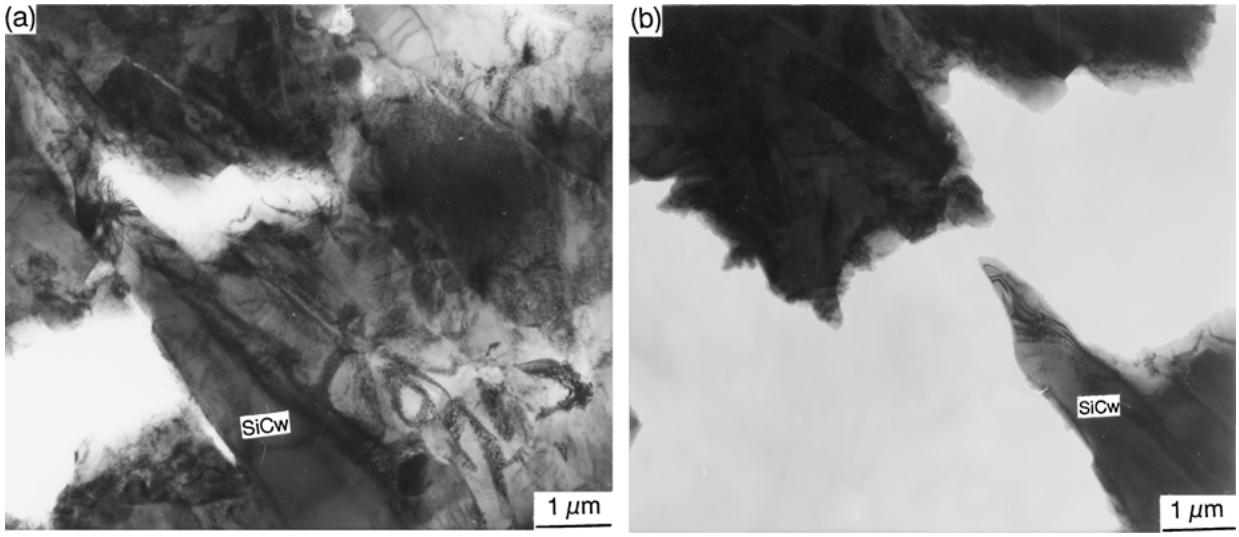

Figure 8 Interaction between crack and SiC whisker. (a) Crack by-passing the middle part of a whisker and (b) pulling out of the SiC whisker.

main cracks stop propagating before final failure, only one of them prevails, which leads to the final failure of the composite. Fig. 9 shows a main crack which stop propagating before the failure of the specimen. It can be seen clearly that crack propagates along the matrix near the SiCw-AZ91 interface, and the fracture surface seems to be flat, which may be associated with the low ductility of the AZ91 matrix alloy.

Fig. 10 shows the main crack propagation path in the composite which leads to the final failure of the foil. It can be seen that local thinning and microcracks initiate in the matrix ahead of the main crack, as shown in Fig. 10a. These local thinning and microcracks usually initiate in the matrix near the whiskers. Dislocation pile-up can be observed around the local thinning region. On further loading, the main crack connects with the microcraks ahead, and the main crack propagates, as shown in Fig. 10b. Crack propagates mainly through the matrix. There is less evidence of whisker cracking and interface debonding, indicating that the SiCw-Mg interfacial bond is relatively strong.

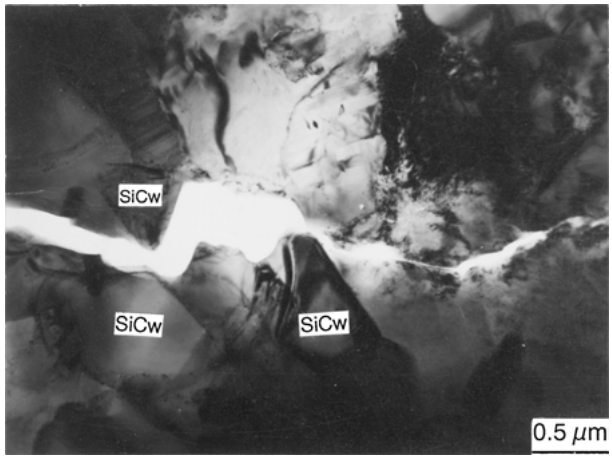

Figure 9 Crack propagation path during *in-situ* TEM tensile of SiCw/AZ91 composite.

4. Discussion

It is generally accepted that slip on the {0001}basal plane with a $\langle 11\bar{2}0\rangle$ Burgers vector and $\{10\bar{1}2\}$ twinning are the principal deformation models in the solution treated AZ91 magnesium alloy [31]. In the solution treated SiCw/AZ91 composite after straining, complex dislocation tangles can be observed, which may be resulted from the cross slip on the prism planes combined with basal slip on the basal planes. Although several twins can be observed in the matrix of the as-solutionized SiCw/AZ91 composite, twinning can hardly be observed during the deformation of the composite, indicating that the $\{10\bar{1}2\}$ twinning may be suppressed by the addition of SiC whiskers. The mechanism by which SiC whiskers suppress the twin formation is not clear at present.

The deformation in the SiCw/AZ91composite is heterogeneous. On straining, dislocations are generated mainly at the SiCw-AZ91 interface. This indicates that plastic deformation takes place at first in the magnesium matrix adjacent to the SiCw-Mg interfaces, because of the local stress concentration in these regions. Similar observations during *in-situ* TEM straining on SiCw-Al composites have been reported [9, 10].

Due to the limited slip systems in hexagonal closed packed magnesium alloys, the local stress concentration in the magnesium alloys can not be easily relaxed by plastic deformation compared with aluminum alloys. Consequently, a large number of microcracks are initiated at the stress concentration sites in the SiCw/AZ91 composite when the macroscopic strain level is low. The microcracks generally initiate in the matrix adjacent to the SiCw-AZ91 interface, especially in the matrix near the SiC whisker ends. The microcrack formation near the whisker ends has been commonly accepted as a major fracture initiation process in SiC whisker reinforced aluminum matrix composite [4, 9], because of the severe stress concentration at the whisker ends [32]. In addition, microcracks also initiate in the matrix in the whisker-rich regions since the larger deformation in these regions, which is the same as that in SiCw/Al composites [9].

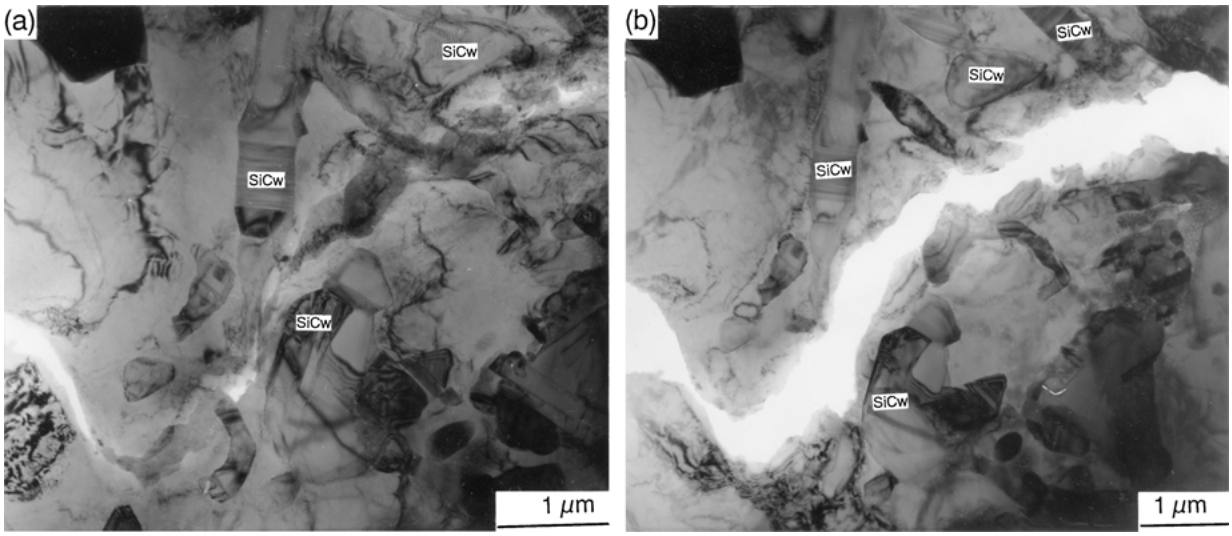

Figure 10 Propagation of main crack in SiCw/AZ91 composite. (a) Local thinning and microcracks formed in front of main crack and (b) path of main crack propagation.

As previously observed in SiCw-A1 composites, SiC whiskers in the composites play important roles in impeding crack propagation [4, 9, 10]. The dislocations piling up at the SiCw-Mg interface force the crack to change its propagation direction. When a crack meets a whisker parallel to the crack, the crack will propagate along the near-interface region of one side of the whisker. If a crack meets a whisker perpendicular to the crack, the whisker will be pulled out. Such effects slow down the crack growth. In addition to the whiskers, twins formed in the solution treated SiCw/AZ91 composite also impede crack propagation. When a running crack interacts with a twin, its path changes into a direction along the twin-matrix interface. Same behavior was observed in the magnesium alloys [33].

Although whiskers and twins can prohibit the crack propagation, local thinning and microcracks usually occur in the vicinity of the whiskers and twins because of stress concentration in these regions. Therefore, the whiskers and twins, on the other hand, accelerate the crack initiation and growth. On the whole, the latter effect is more evident.

From the above observation and analysis, the failure process of the SiCw/AZ91 composite during *in-situ* TEM straining is as follows: on straining, plastic deformation takes place in the local stress concentration regions at first, local thinning occurs in the vicinity of whiskers. Then local thinning develops into microcracks. Upon further straining, these microcracks linked with each other together, and then connected to the main crack, leading to the growth of main crack. The various stages of crack initiation and crack propagation can not be separated easily, because during the crack propagation many new cracks are initiated. Usually more than one main crack propagates through the foil in direction approximately perpendicular to the applied tensile stress. Finally, one of them prevails and the ultimate fracture surface is formed when the composite fails catastrophically.

The crack path is almost entirely in the matrix away from the interface, suggesting a matrix-controlled fracture mechanism in the foil specimen of SiCw/AZ91 composite. Due to the plane stress condition of the TEM foil specimen, the observed failure mechanisms may not be identical to those which occur in the bulk material which is in a stress condition closer to plane strain [8]. Under the plane strain condition, both the tensile stress at the reinforcement-matrix interface and the dilatational stress in the matrix are increased [34]. The increased dilatational stress in the matrix may lower the macroscopic tensile stress required to form microcracks in the magnesium matrix, and the increased tensile stresses at the SiCw-Mg interface may lead to interfacial decohesion and fracture of the SiC whiskers in bulk specimens. Therefore, the validity of the *in-situ* TEM investigation as representations of failure processes occurring in the bulk of SiCw/AZ91 composite is checked with the conventional SEM tensile fractographic results of the composite. Consistent with the observations during the *in-situ* TEM tensile test, the amount of SiC whiskers detected at the SEM fracture surface of bulk tensile specimen is quite small in comparison to the volume fraction of SiC whisker in the SiCw/AZ91 composite. Furthermore, less evidence of interfacial decohesion and fracture of SiC whisker on the SEM fracture surface was found. In view of these observations, interfacial decohesion and fracture of SiC whisker are unlikely to play a major role in the failure of the bulk SiCw/AZ91 composite.

Thus it appears that the failure characteristics observed during *in-situ* TEM strain are in qualitative agreement with that occurring in the bulk SiCw/AZ91 composite, the observed features during *in situ* TEM straining can be considered to be valid to illustrate the failure behavior of the SiCw/AZ91 composite.

Since the crack mainly propagates through the matrix and along near-interface region, much less interface decohesion can be observed, the strength of the Mg─SiC interface is suggested to be relatively strong, higher than the yield stress of the magnesium matrix. The previous research by the present author [35] indicates that several kinds of orientation relationships at the SiCw-AZ91 interface are observed in squeeze cast SiCw/AZ91 composite, which resulted

from the solidification of molten Mg at the different surface planes of SiC whisker. High interfacial bond strength exists in these semi-coherent interfaces. Furthermore, some discrete nanocrystalline MgO particles with a size of 20 nm or less are observed at the SiCw/AZ91 interfaces [36], which were formed during the fabrication of the composite by chemical reaction of molten Mg with binder in the SiCw preform. The fine discrete interfacial MgO reaction products can also increase the whisker-matrix interfacial bonding strength. Therefore, the SiCw-AZ91 interface is strong enough, no interfacial debonding can be observed both in the thin foils and bulk specimens of the SiCw/AZ91 composite.

The fracture mechanism of the SiCw/AZ91 composite is mainly controlled by the matrix because of the crack path mainly in the matrix of the composite. The addition of SiC whisker does not modify qualitatively the failure micromechanisms in the magnesium matrix alloy. However, the severe local stress concentration generated near the whiskers can not be relaxed by the matrix, which results to the early initiation of micorcracks, so the ductility of the composite is quite lower than the matrix alloy. Even under the solution treated condition, the ductility of the SiCw/AZ91 composite is lower than that of as-cast SiCw/Al composites [10], because of the low inherent ductility of the matrix magnesium alloy with limited active slip systems. Therefore, the low inherent ductility of the matrix magnesium alloy and the local stress concentration because of the addition of the whiskers are responsible for the poor ductility of the SiCw/AZ91composite.

5. Conclusions

The *in-situ* TEM straining technique used in this study is useful for investigating the deformation and fracture behavior of SiCw/AZ91 composite. The important results are the following:

1. The deformation is very localized in the SiCw/AZ91 composite. Local thinning and microcraks take place predominately in the matrix near SiCw-AZ91 interface regions. The main crack advances by linkage with microcracks, leading to the final failure of the composite.

2. The SiC whiskers and twins, on the one hand, impede the crack propagation; on the other hand, microcracks occur easily in the vicinity of the whiskers and twins because of stress concentration in these regions. Overall, the whiskers and twins accelerate the crack initiation and growth.

3. The crack mainly propagates through the matrix and along near-interface region. A magnesium layer can be found adhering to the SiC whiskers. The strength of the Mg-SiC interface is relatively strong, higher than the yield stress of the magnesium matrix.

4. The fracture mechanism of the SiCw/AZ91 composite is matrix-controlled. Low inherent ductility of the matrix magnesium alloy and the local stress concentration because of the addition of the whiskers are responsible for the poor ductility of the composite.

References

1. A. F. WHITEHOUSE and T. W. CLYNE, *Acta Metall. Mater.* **41** (1993) 1701.
2. C. G. KANG and Y. H. SEO, *J. Mater. Process Tech.* **61** (1996) 241.
3. G. J. MAHON, J. M. HOWE and A. K. VASUDEVAN, *Acta Metall.* **38** (1990) 1503.
4. C. S. LEE, Y. H. KIM, T. LIM and K. S. HAN, *Scr. Metall.* **25** (1991) 613.
5. M. MANOHARAN and J. J. LEWANDOWSKI, *ibid.* **23** (1989) 1801.
6. J. A. VREELING, V. OCELÝ'K, G. A. HAMSTRA, Y. T. PEI and J. HOSSON, *Scr. Mater.* **42** (2000) 589.
7. P. M. MUMMERY and B. DERBY, *J. Mater. Sci.* **29** (1994) 5615.
8. S. H. DOONG, T. C. LEE, I. M. ROBERTSON and H. K. BIRNBAUM, *Scr. Metall.* **23** (1989) 1413.
9. Z. R. LIU, D. Z. WANG, C. K. YAO, J. LIU and L. GENG, *Mater. Sci. Eng.* **A189** (1994) 235.
10. Y. H. LIU, Z. G. WANG and Z. Y. MA, in "Strength of Materials," edited by Okikawa (The Japan Institute of Metals, 1994) p. 509.
11. Y. BRECHET, J. D. EMBURY, S. TAO and L. LUO, *Acta Metall. Mater.* **39** (1993) 1781.
12. A. J. REEVES, H. DUNLOP and T. W. CLYNE, *Metall. Trans.* **23** (1991) 970.
13. D. J. LLOYD, H. LAGACE, A. MCLEOD and P. L. MORRIS, *Mater. Sci. Eng.* **107A** (1989) 73.
14. S. CHANG, H. TEZUKA and A. KAMIO, *Materials Transaction, JIM.* **38** (1997) 18.
15. A. LUO, *Metall. Mater. Trans.* **26A** (1994) 2445.
16. K. PURAZRANG, K. U. KAINER and B. L. MORDIKE, *Composites* **22** (1991) 456.
17. K. PURAZRANG, P. ABACHI and K. U. KAINER, *Composites Eng.* **3** (1993) 489.
18. A. MARTIN and J. LLORCA, *Mater. Sci. Eng.* **A201** (1995) 77.
19. K. SOHN, K. EUH, S. LEE and I. PARK, *Metall. Mater. Trans.* **29A** (1998) 2543.
20. J. S. KIM, M. SUGAMATA and J. KANEKO, *J. Japan Inst. Metals* **55** (1991) 521.
21. S. RYU, J. KANEKO and M. SUGANUMA, *ibid.* **61** (1997) 1160.
22. M. Y. ZHENG, K. WU and C. K. YAO, *Mater. Sci. Eng. A* **A318** (2001) 50.
23. K. U. KAINER and B. L. MORDIKE, *Metall.* **44** (1990) 438 (in Germany).
24. B. A. MIKUCKI, W. E. MERCER and W. G. GREEN, *Light Metal Age* **6** (1990) 12.
25. T. E. WILKS, *Adv. Mater. Processes* **8** (1992) 27.
26. T. WADA, T. SHINKAWA, S. KAMADO and Y. KOJIMA, *J. Japan Inst. Light Metals* **45** (1995) 510.
27. B. Zhang, *et al.*, in "Nonferrous Alloys and Their Heat Treatment" (Defense Industry Press, Beijing, 1981) p. 155 (in Chinese).
28. Tokai SiC whisker catalog, Tokai Carbon Co., Ltd. Japan.
29. ASM, in "ASM Handbook, Properties and Selection: Nonferrous Alloys and Special-Purpose Materials," Vol. 2 (ASM International, 1995) p. 496.
30. M. VOGELSANG, R. J. ARSENAULT and R. M. FISHER, *Metall. Trans.* **17A** (1986) 379.
31. J. B. CLARK, *Acta Metall.* **16** (1968) 141.
32. S. R. NUTT and J. M. DUVA, *Scr. Metall.* **20** (1986) 1055.
33. J. V. PLANKEN and J. M. DUPOY, *Phy. Status Solidi* **39** (1970) 9.
34. T. CHRISTMAN, A. NEEDLEMAN, S. NUTT and S. SURESH, *Mater. Sci. Eng.* **A107** (1989) 49.
35. M. Y. ZHENG, K. WU, C. K. YAO, T. SATO, H. TEZUKA, A. KAMIO and D. LI, *Mater. Letters* **41** (1999) 57.
36. M. Y. ZHENG, K. WU and C. K. YAO, *Mater. Letters* **47** (2001) 118.

Received 29 July 2002
and accepted 3 April 2003